

Effect of Strain Rate on Hot Ductility Behavior of a High Nitrogen Cr-Mn Austenitic Steel



ZHENHUA WANG, QING MENG, MINGGUI QU, ZEAN ZHOU, BO WANG,
and WANTANG FU

18Mn18Cr0.6N steel specimens were tensile tested between 1173 K and 1473 K (900 °C and 1200 °C) at 9 strain rates ranging from 0.001 to 10 s⁻¹. The tensile strained microstructures were analyzed through electron backscatter diffraction analysis. The strain rate was found to affect hot ductility by influencing the strain distribution, the extent of dynamic recrystallization and the resulting grain size, and dynamic recovery. The crack nucleation sites were primarily located at grain boundaries and were not influenced by the strain rate. At 1473 K (1200 °C), a higher strain rate was beneficial for grain refinement and preventing hot cracking; however, dynamic recovery appreciably occurred at 0.001 s⁻¹ and induced transgranular crack propagation. At 1373 K (1100 °C), a high extent of dynamic recrystallization and fine new grains at medium strain rates led to good hot ductility. The strain gradient from the interior of the grain to the grain boundary increased with decreasing strain rate at 1173 K and 1273 K (900 °C and 1000 °C), which promoted hot cracking. Grain boundary sliding accompanied grain rotation and did not contribute to hot cracking.

DOI: 10.1007/s11661-015-3308-3

© The Minerals, Metals & Materials Society and ASM International 2015

I. INTRODUCTION

NITROGEN is an effective solid-solution strengthener, a pitting resistance enhancer, and also a strong austenite stabilizer.^[1] Owing to these beneficial effects of nitrogen, high nitrogen Cr-Mn austenitic steels possess an interesting combination of mechanical, chemical, and physical properties: high strength and toughness, good corrosion resistance, and low magnetic susceptibility.^[1,2] These steels have been widely used in engineering^[3] with a typical example being heavy retaining rings.^[4] However, high nitrogen Cr-Mn austenitic steels are sensitive to hot cracking during the hot working process, leading to high production costs and low efficiency.^[4-6]

Several process variables must be considered to avoid hot cracking in steel, such as the preheating temperature, deformation temperature, and strain rate. An excessively high preheating temperature results in a large initial grain size, which reduces the hot ductility of the steel.^[5,7] A higher preheating temperature also leads to the formation of delta ferrite and promotes the nucleation, propagation, and linkage of cracks.^[6] A high

deformation temperature is beneficial for dynamic recrystallization (DRX),^[8] which allows high hot ductility to be achieved.^[9] In contrast, at lower deformation temperatures, Cr₂N may precipitate and have a negative effect on the hot ductility.^[9,10] Although process parameters such as the preheating and deformation temperatures have been well studied, few studies have focused on the effect of strain rate on the hot ductility behavior of high nitrogen Cr-Mn austenitic steels.

The strain rate is known to have a pronounced effect on the hot ductility of metallic materials. In AZ31 alloys, the elongation at fracture increases with decreasing strain rate.^[11,12] Similar trends have been observed in Csf/AZ91D^[13] and AZ81.^[14] The effect of strain rate on hot ductility of steels is more complex. No obvious strain rate effect is observed in super 304H austenitic steel.^[15] However, the equivalent fracture strain increases with decreasing strain rate for 30Cr2Ni4MoV steel^[16] and 2205 steel.^[17] In contrast, a low strain rate decreases the hot ductility of C-Mn-Nb-Al steel^[18] and Cr17Mn6Ni4Cu2N steel.^[19] In other austenitic steels, a detrimental effect of low strain rate on hot ductility has also been observed.^[20-22]

Electron backscatter diffraction (EBSD) is a powerful technique to investigate cracking in crystalline materials. It has been widely used in studies concerning fatigue cracking,^[23] tensile cracking,^[24] forging cracking,^[5] and corrosion cracking,^[25] among others. Detailed crystallographic information on the mechanism of crack nucleation, crack propagation, and crack barriers can be obtained. The objectives of the present study are to reveal the strain rate effect (at strain rates from 0.001 to 10 s⁻¹) on the hot ductility behavior of a high nitrogen Cr-Mn austenitic steel using EBSD, and to apply the

ZHENHUA WANG, Associate Professor, is with the School of Mechanical Engineering, Yanshan University, Qinhuangdao 066004, P.R. China, and also with the Hebei Iron & Steel Technology Research Institute, Shijiazhuang 050023, P.R. China, and State Key Laboratory of Metastable Materials Science and Technology, Yanshan University, Qinhuangdao 066004, P.R. China. Contact e-mail: wangzhenhua@ysu.edu.cn QING MENG, Student, is with the School of Mechanical Engineering, Yanshan University. MINGGUI QU, Research Assistant, ZEAN ZHOU and BO WANG, Students, and WANTANG FU, Professor, are with the State Key Laboratory of Metastable Materials Science and Technology, Yanshan University.

Manuscript submitted June 26, 2015.

Article published online January 4, 2016

EBSD technique to investigate hot ductility in austenitic steel.

II. EXPERIMENTAL

The investigated 18Mn18Cr0.6N steel was melted in a vacuum electric furnace (80 t) and then electroslag remelted (10 t). Its chemical composition was (wt pct): 0.084 C, 17.9 Mn, 18.06 Cr, 0.62 N, 0.46 Si, 0.2 Ni, 0.009 P, 0.002 S, and balance Fe. Small slabs were cut from the ingot and rolled at 1373 K (1100 °C). The total true strain during rolling was ~ 2 . The rolled slabs were heat treated at 1473 K (1200 °C) for 1 hour to obtain an average grain size of 210 μm . The grain size was measured using the line intercept method.

Specimens ($\Phi 6 \times 120$ mm) were cut parallel to the rolling direction. Hot tensile tests were conducted on a Gleeble-3500 simulator. The specimens were preheated at a rate of 10 K s^{-1} ($^{\circ}\text{C s}^{-1}$) to 1173 K, 1273 K, 1373 K, and 1473 K (900 °C, 1000 °C, 1100 °C, and 1200 °C). Thereafter, tensile tests were performed at 0.001, 0.003, 0.01, 0.03, 0.1, 0.3, 1, 3, and 10 s^{-1} . The specimens were then deformed to a strain of 0.2 to 1. A gage length of 12 mm was used to determine the strain. Some specimens were tensioned to fracture, whereas others were not. The hot ductility was quantified in terms of the reduction in area (RA) at fracture.

Unbroken specimens were sectioned parallel to the direction of tension. The observation area was situated in the center of the specimen in the deformed region. EBSD analyses were performed using TSL-OIM-Analysis software to investigate specimens with a spatial resolution of 0.3 to 2 μm and misorientation detection limit of 1 deg. The crystal orientation maps displayed high-angle grain boundaries (GBs) (misorientations ≥ 15 deg, shown as black lines), twin boundaries (shown as white lines), and low-angle GBs ($2 \text{ deg} \leq$ misorientations < 15 deg, shown as gray lines). Points with confidence indices lower than 0.1 were filtered and shaded black (cracks exhibit low confidence indices). The GB profile and differences in crystallographic

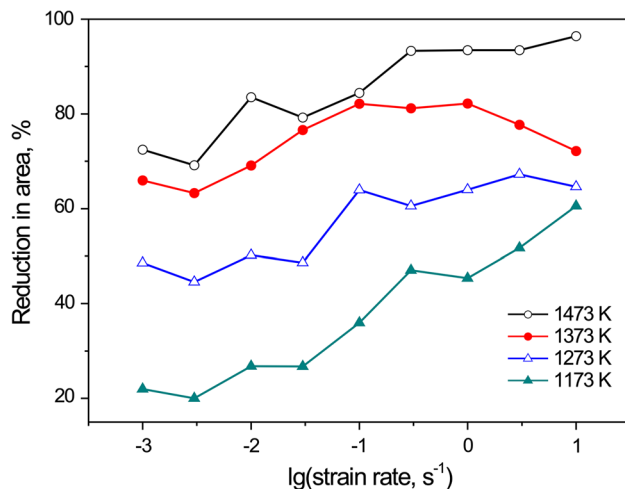


Fig. 1—Dependence of RA on the strain rate.

orientation of the specimens after the hot tensile tests were plotted as inverse pole figure (IPF) maps, kernel average misorientation (KAM) maps, and Taylor factor maps. The first nearest neighbors at the perimeter within 5 deg were used to determine the KAM.

III. RESULTS

A. Hot Ductility

The dependence of RA on the strain rate is shown in Figure 1 under different deformation conditions. The effect of strain rate varies markedly with deformation temperature. At 1473 K (1200 °C), the RA increases with increasing strain rate, exceeding 90 pct above 0.3 s^{-1} . At 1373 K (1100 °C), the RA obtained at 0.001 s^{-1} is about 65 pct. A higher RA of about 80 pct is observed within the strain rate range of 0.03 to 1 s^{-1} . Beyond this range, the RA decreases with increasing strain rate. At 1273 K (1000 °C), the RA is around 45 pct at 0.001 to 0.03 s^{-1} and is around 60 pct at 0.1 to 10 s^{-1} . The most obvious effect of strain rate is at 1173 K (900 °C), at which the RA increases with increasing strain rate from 21 to 60 pct.

Figure 2 shows the tensile flow curves. 18Mn18Cr0.6N steel is a strain-rate-sensitive material. For most deformation conditions, the deformation resistance increases with strain rate. The elongation at fracture also increases with strain rate. To observe the difference in microstructure evolution between specimens tensioned at different strain rates, three strain rates of 0.001, 0.1, and 10 s^{-1} were selected. The corresponding flow curves are represented by the solid lines in Figure 2; the vertical dashed line denotes the corresponding tensile strain. The tensile strained microstructures are shown in Sections III-B through III-E.

B. Tensile Strained Microstructure at 1473 K (1200 °C)

The results for the specimen tensioned at 1473 K (1200 °C) and 10 s^{-1} to a strain of 0.4 are shown in Figure 3. In the IPF map (Figure 3(a)), it can be seen that partial DRX occurred and most fine grains are located at triple junctions. Only a small number of low-angle GBs are observed. A 10- μm -long crack appears and is marked by the number 1. Detailed views of the crack are shown in Figures 3(b) through (d). To observe the KAM value distribution, the low-angle GBs are not plotted in the KAM map (Figure 3(c)). The KAM values around the crack are nonuniform and are high in the grains with high Taylor factors on the left side of the crack (Figures 3(c) and (d)). The sharp angle of the crack appears to be along a GB.

When the strain rate is lowered to 0.1 s^{-1} , more fine cracks appear in the specimen (Figure 4(a)), as marked by the numbers. Their lengths are about 50 μm . It should be noted that the magnification is lower in this case than in Figure 3. From their shapes, it is evident that the cracks propagated parallel to the tensile direction. In the IPF map (Figure 4(b)), it can be seen that almost full DRX occurred in the specimen with

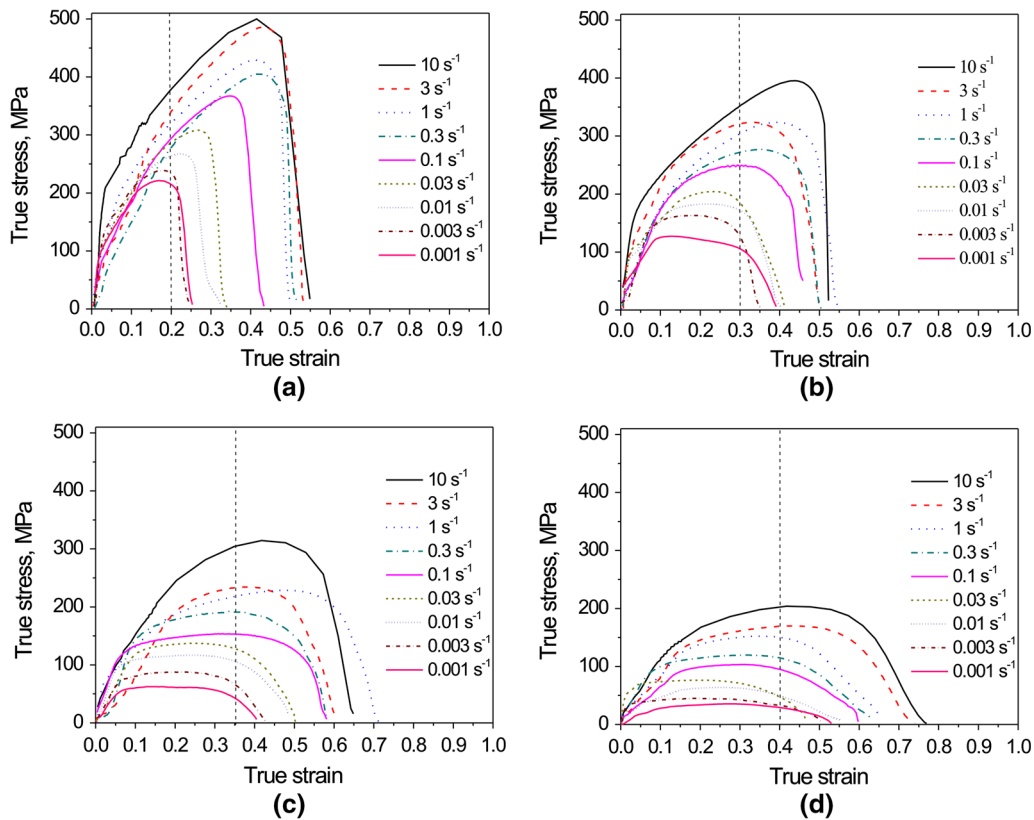


Fig. 2—Tensile flow curves of 18Mn18Cr0.6N steel. (a) 1173 K (900 °C); (b) 1273 K (1000 °C); (c) 1373 K (1100 °C); (d) 1473 K (1200 °C).

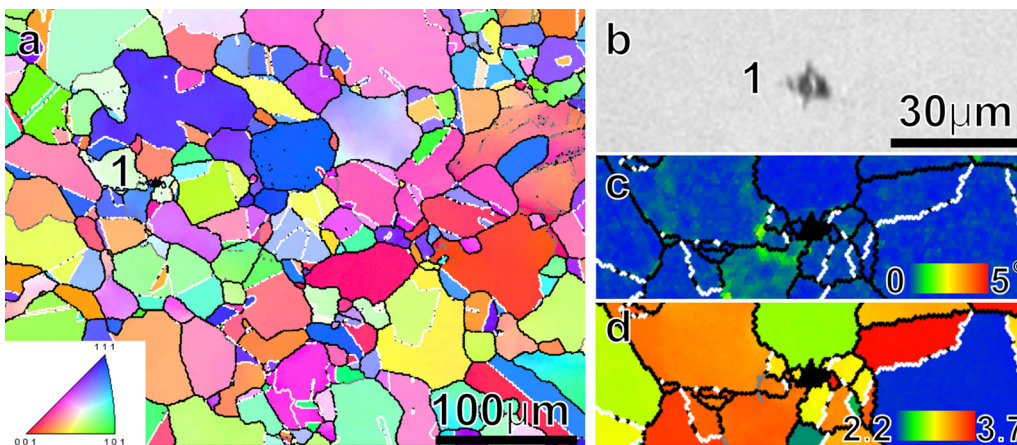


Fig. 3—(a) IPF map of the specimen tensioned at 1473 K (1200 °C) and 10 s^{-1} to a strain of 0.4; (b) detailed scanning electron microscopy (SEM) image of (a); (c) corresponding KAM map; (d) Taylor factor map of (b). The horizontal direction is the tensile direction in this and the following figures.

cracks located in the DRX region. Figures 4(c) and (d) show the detailed KAM and Taylor factor maps of the cracks. The KAM values surrounding crack 1 are high, similar to those in Figure 3(c). In contrast, the KAM values next to crack 2 are very low. Branching occurs in both cracks 4 and 5, with branching occurring toward the interior of the grains with high Taylor factors for crack 4, and along the GBs with crack 5. From the data presented in Figure 4, it can be seen that crack edges with low curvature occur primarily next to grains with

low Taylor factors, and vice versa. This can be explained by the inhibition effect of grains with lower Taylor factors on crack propagation.^[5]

When the strain rate is lowered to 0.001 s^{-1} , the microstructure is quite different to those presented in Figures 3 and 4. Large cracks are apparent in the SEM image (Figure 5(a)). Many low-angle GBs are found in the IPF map (Figure 5(b)). These low-angle GBs and dislocation walls are mainly located in grains with low Taylor factors (Figures 5(c) and (d)). We consider that

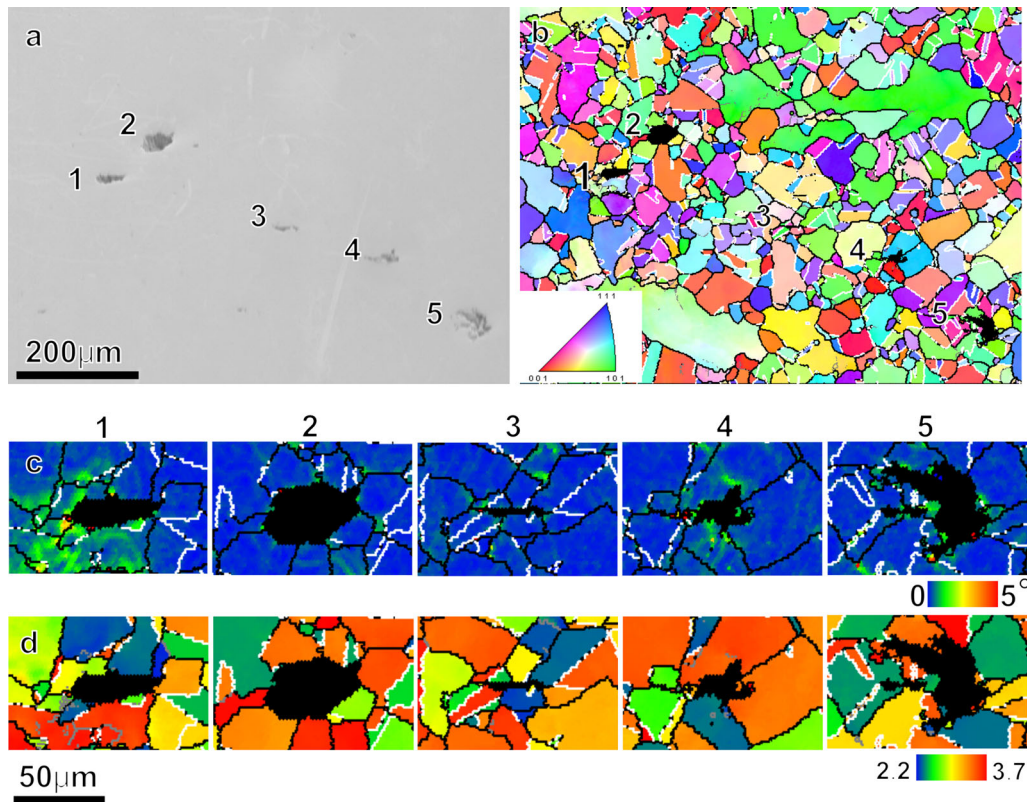


Fig. 4—(a) SEM image of the specimen tensioned at 1473 K (1200 °C) and 0.1 s^{-1} to a strain of 0.4; (b) corresponding IPF map; (c) detailed KAM map; and (d) Taylor factor map of the cracks.

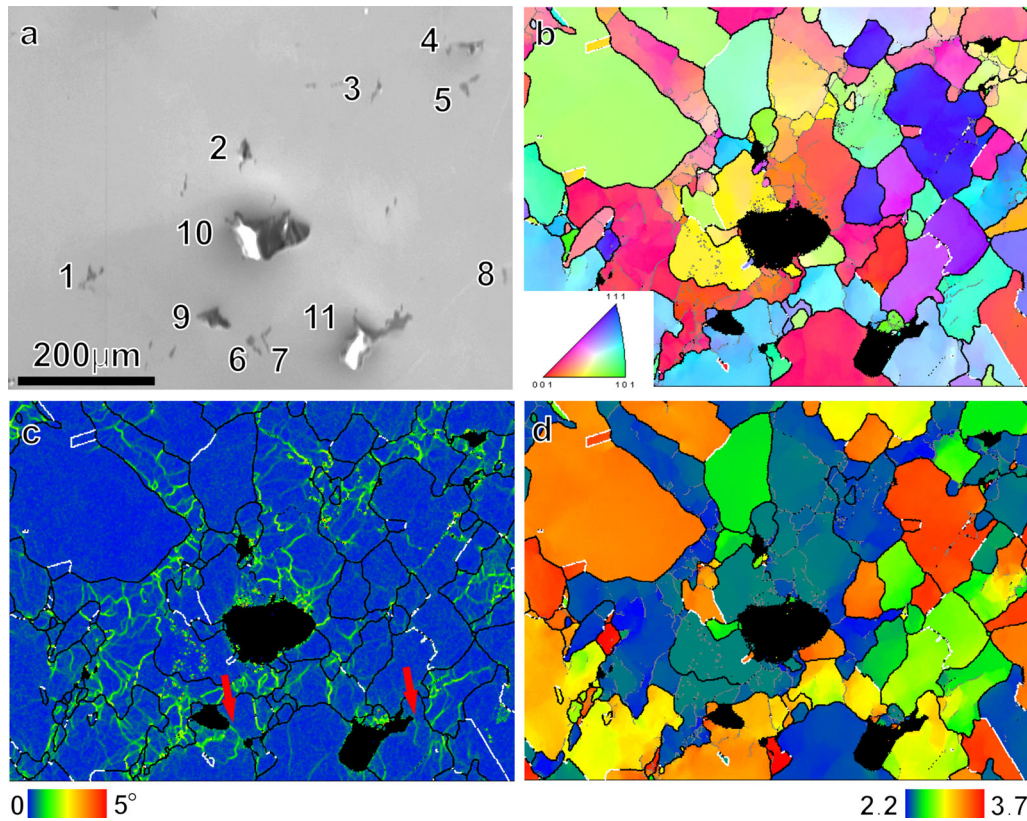


Fig. 5—(a) SEM image of the specimen tensioned at 1473 K (1200 °C) and 0.001 s^{-1} to a strain of 0.4; (b) corresponding IPF map; (c) KAM map; and (d) Taylor factor map.

the small crack is newly formed and the large crack is a propagated crack. The nucleation sites are mainly at high-angle GBs (cracks 1–8). It is interesting to note that cracks propagate along low-angle GBs or dislocation walls (indicated by the red arrows, cracks 9, and 11), which is quite different to previously reported observations.^[5,9,10]

C. Tensile Strained Microstructure at 1373 K (1100 °C)

Figure 6 shows the results for the specimen tensioned at 1373 K (1100 °C) and 10 s^{-1} to a strain of 0.35. Partial DRX occurs and new grains are mainly located at triple junctions and existing GBs (Figure 6(a)). No cracks are observed and sliding bands with misorientation angles larger than 2 deg appear in some grains. A small grain appears within the parent grain, as indicated by the red ellipse. In the KAM map (Figure 6(b)), it is evident that a DRX grain is present with a low dislocation density. Intragranular DRX occurs at high strain rates and is usually associated with large particles, such as inclusions.^[8] It should be noted that the large grains with low KAM values in Figure 6(b) are not DRX grains.

The results for the specimen tensioned at 0.1 s^{-1} are shown in Figure 7. The extent of DRX is greater than that in Figure 6. In the parent grains, no obvious sliding lines can be found and the KAM values are lower than those in the grains with sliding lines in Figure 6(b). At higher strain rate, the strain distribution appears to be more uniform; that is, the strain dislocation gradient from the interior of the grain to the GB is smaller. Two cracks appear in the DRX region near the parent grains. For crack 1, both the upper front and middle bend are next to regions with high KAM values. For crack 2, the pointed end is also directed toward a region with high KAM values.

When the strain rate is lowered to 0.001 s^{-1} , many cracks appear (Figure 8(a)). The extent of DRX (Figure 8(b)) is greater than that in Figures 6 and 7. In the deformed parent grains, very few twins can be found. This means that the nucleation of DRX grains is mainly accompanied by the evolution of low-angle

GBs.^[7] The KAM values are high in this specimen, both in the parent and DRX grains (Figure 8(c)). Cracks 2 and 9 branch when they meet the DRX grains. The propagation of crack 5 appears to be transgranular, similar to that for the crack in Figure 5.

D. Tensile Strained Microstructure at 1273 K (1000 °C)

The RA of the specimen tensioned at 0.1 s^{-1} is similar to that at 10 s^{-1} at 1273 K (1000 °C). Therefore, the deformed microstructure of the latter was not examined. Figure 9 shows the results for the specimen tensioned at 0.1 s^{-1} to a strain of 0.3. The parent grains are elongated and some twins are curved (Figure 9(a)). Very few DRX grains were observed. Low-angle GB and high KAM values appear along the existing grain and twin boundaries (Figure 9(b)). It is noteworthy that twin boundaries are also potential DRX nucleation sites.^[26]

Figure 10 shows the results for the specimen tensioned at 0.001 s^{-1} . Many fine cracks appear in the SEM image (Figure 10(a)). In the IPF map (Figure 10(b)), fine DRX grains form along the existing GBs. This kind of structure is referred to as a necklace DRX.^[27] Although DRX consumes damage and restores ductility along the existing GBs, cracks still appear along these boundaries. Cracks 1 to 6 are small and are located between the parent grains and the necklace regions. Cracks 7 to 11 are large and are located between the large parent grains.

E. Tensile Strained Microstructure at 1173 K (900 °C)

Figure 11 shows the results for the specimen tensioned at 1173 K (900 °C) and 10 s^{-1} to a strain of 0.2. Because of the low strain, grains were not appreciably elongated (Figure 11(a)). In some grains, there are slip bands for which the corresponding KAM values are high and uniform (Figure 11(b)). No cracks are observed in this case.

When the strain rate is reduced to 0.1 s^{-1} (Figure 12), high KAM values appear mainly along the GBs instead of being uniformly distributed throughout the whole grain. No cracks are observed in this case either.

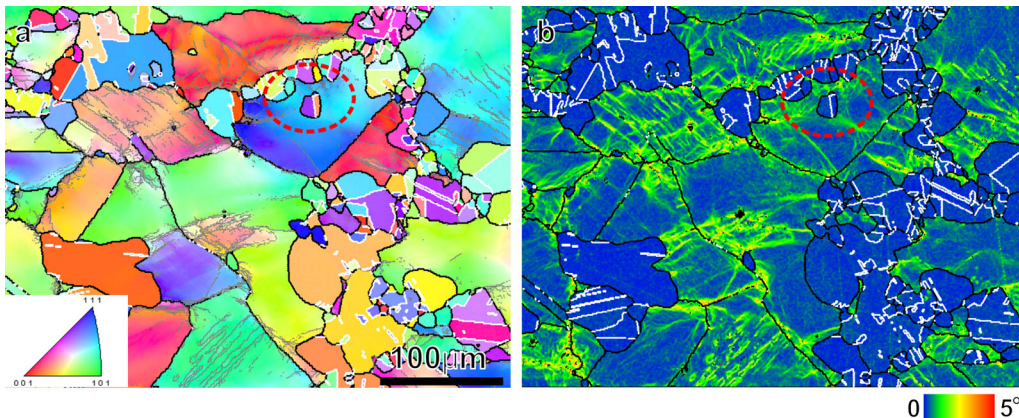


Fig. 6—(a) IPF map of the specimen tensioned at 1373 K (1100 °C) and 10 s^{-1} to a strain of 0.35 and (b) corresponding KAM map.

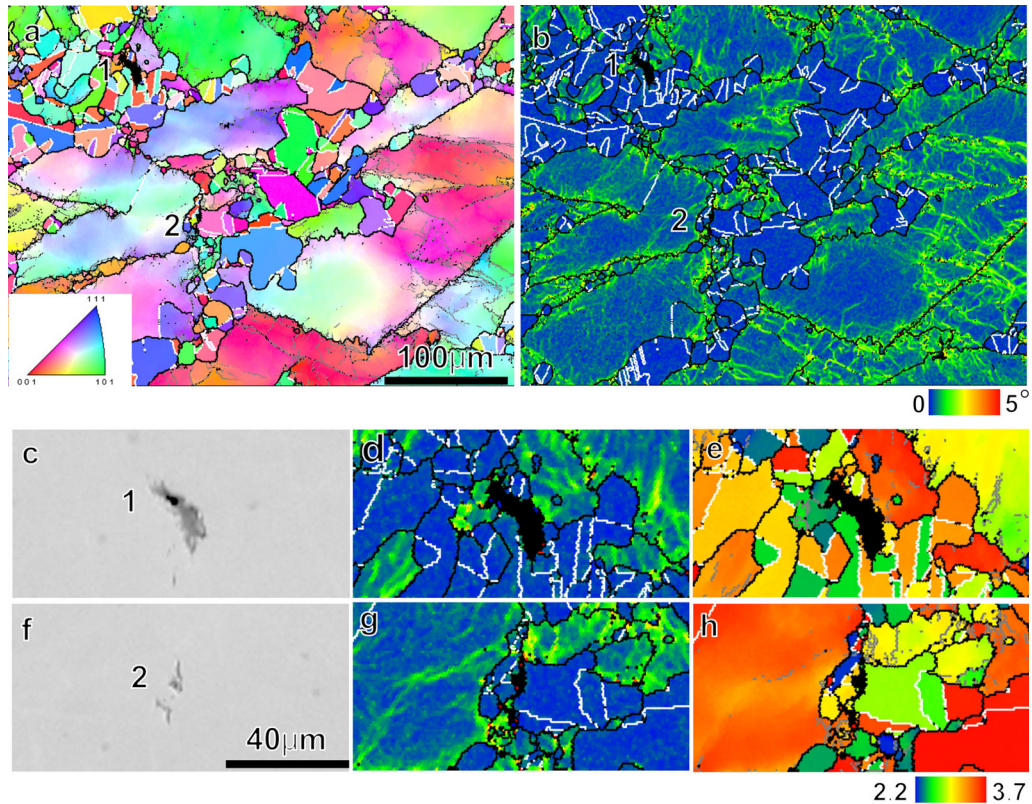


Fig. 7—(a) IPF map of the specimen tensioned at 1373 K (1100 °C) and 0.1 s^{-1} to a strain of 0.35; (b) corresponding KAM map; (c) detailed SEM image of crack 1; (d) corresponding KAM map and (e) Taylor factor map of (c); (f) detailed SEM image of crack 2; (g) corresponding KAM map and (h) Taylor factor map of (f).

At a strain rate of 0.001 s^{-1} , a narrow crack appeared perpendicular to the tension direction (Figure 13) and between grains with high Taylor factors (Figure 13(b)). This is consistent with the results in Reference 5.

IV. DISCUSSION

A. Dynamic Recovery

The stacking fault energy of high nitrogen Cr-Mn austenitic steel is low^[28] and DRX rather than dynamic recovery (DRV) usually occurs during hot deformation. However, in the present study, at very low strain rates (0.001 s^{-1}) and high deformation temperatures [1473 K and 1373 K (1200 °C and 1100 °C)], many low-angle GBs formed (Figure 14) and appreciable DRV occurred (Figures 5 and 8). That is because high temperature and strain enhance the mobility of dislocations. Furthermore, a lower strain rate gives dislocations more time to climb and form dislocation walls and low-angle GBs.

Based on the above results, a schematic illustration of cracking under very low strain rate (*e.g.*, 0.001 s^{-1}) and high temperature [*e.g.*, 1473 K (1200 °C)] was proposed, as shown in Figure 15. The lower the Taylor factor, the “softer” was the grain. In the early tension stage, the strain is higher in grains with low Taylor factors and the dislocation density is also higher. As deformation develops, dislocations become entangled and cell structures are formed. A localized, high-stress region is thus

established at GBs because of the strain incompatibility between large grains and the additional stress generated by the pileup of dislocations. Stress concentration is relieved by cracking; therefore, the crack nucleation sites are located at GBs (Figure 5(b)). It is well established that the boundary mobility increases significantly with increasing misorientation.^[29] Although cracks form at high-angle GBs, they do not readily propagate along high-angle GBs because of the high migration speed. Therefore, cracks initially develop along low-angle GBs and/or dislocation walls, and then transgranular cracks form (cracks 9 and 11 in Figure 5). Because the density of low-angle GBs and dislocation walls is high in grains with low Taylor factors, the crack front directed toward these grains has a lower curvature (cracks 10 and 11 in Figure 5). Therefore, the curvature of the crack front in or toward grains with high Taylor factors is higher.

B. Dynamic Recrystallization

Cracks branch when they meet fine grains (crack 1 in Figure 3, crack 5 in Figure 4, and cracks 2 and 9 in Figure 8) and the extent of branching will be greater in materials with finer grains. Therefore, a smaller grain size is beneficial for achieving high hot ductility.^[5] Finer DRX grains can be obtained at higher strain rates. At 1473 K (1200 °C) and 10 s^{-1} (Figure 3), the DRX grain size around the crack is about $10 \mu\text{m}$, whereas at 0.1 s^{-1} (Figure 4), it is about $31 \mu\text{m}$. This may explain why the

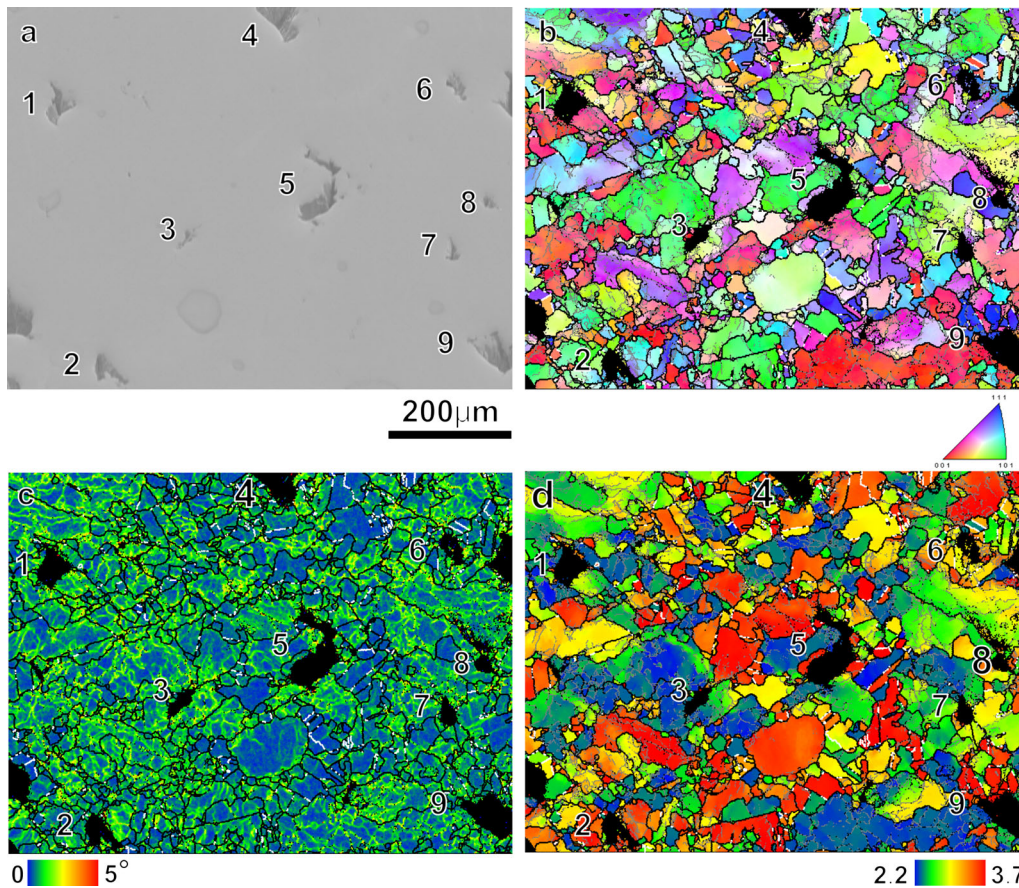


Fig. 8—(a) SEM image of the specimen tensioned at 1373 K (1100 °C) and 0.001 s^{-1} to a strain of 0.35; (b) corresponding IPF map; (c) KAM map; and (d) Taylor factor map.

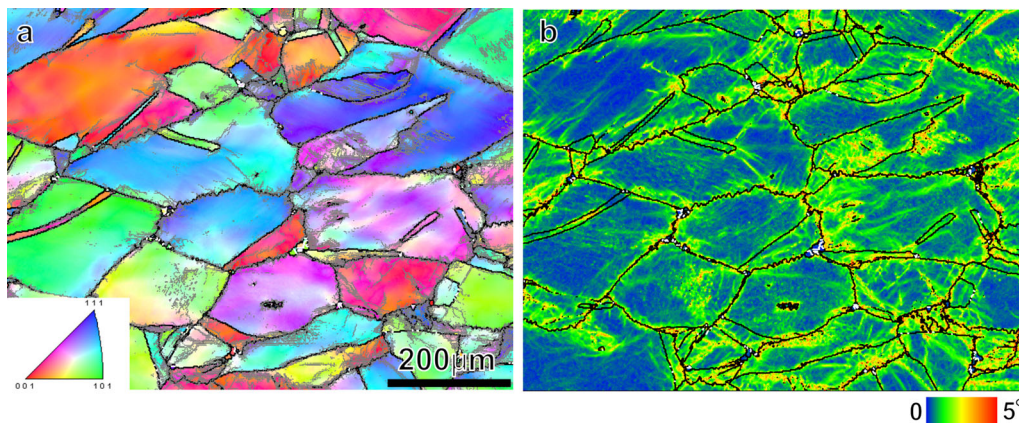


Fig. 9—(a) IPF map of the specimen tensioned at 1273 K (1000 °C) and 0.1 s^{-1} to a strain of 0.3 and (b) corresponding KAM map.

hot ductility of the specimen deformed at 10 s^{-1} is superior to that deformed at 0.1 s^{-1} (Figure 1).

At 1373 K (1100 °C), when the strain rate is higher than 0.1 s^{-1} , the smaller fraction experiences DRX during hot deformation. Since DRX is beneficial to prevent cracking, ductility decreases with strain rate. When the strain rate is lower than 0.1 s^{-1} , lower strain rate leads to coarser DRX grain size and more significant DRV. This may explain why the ductility reaches the maximum at the strain rate of 0.1 s^{-1} (Figure 1).

Although necklace DRX occurred at 0.001 s^{-1} and 1273 K (1000 °C) (Figure 10), the hot ductility is still lower than that obtained at 0.1 s^{-1} . This may be attributed to the strain distribution (*i.e.*, the dislocation density gradient). It is well known that the equicohesive temperature between a GB and the grain interior increases with increasing strain rate. The region near a GB is softer than the grain interior at low strain rates. Therefore, the strain distribution is less uniform and the strain gradient from the grain interior to the GB is larger

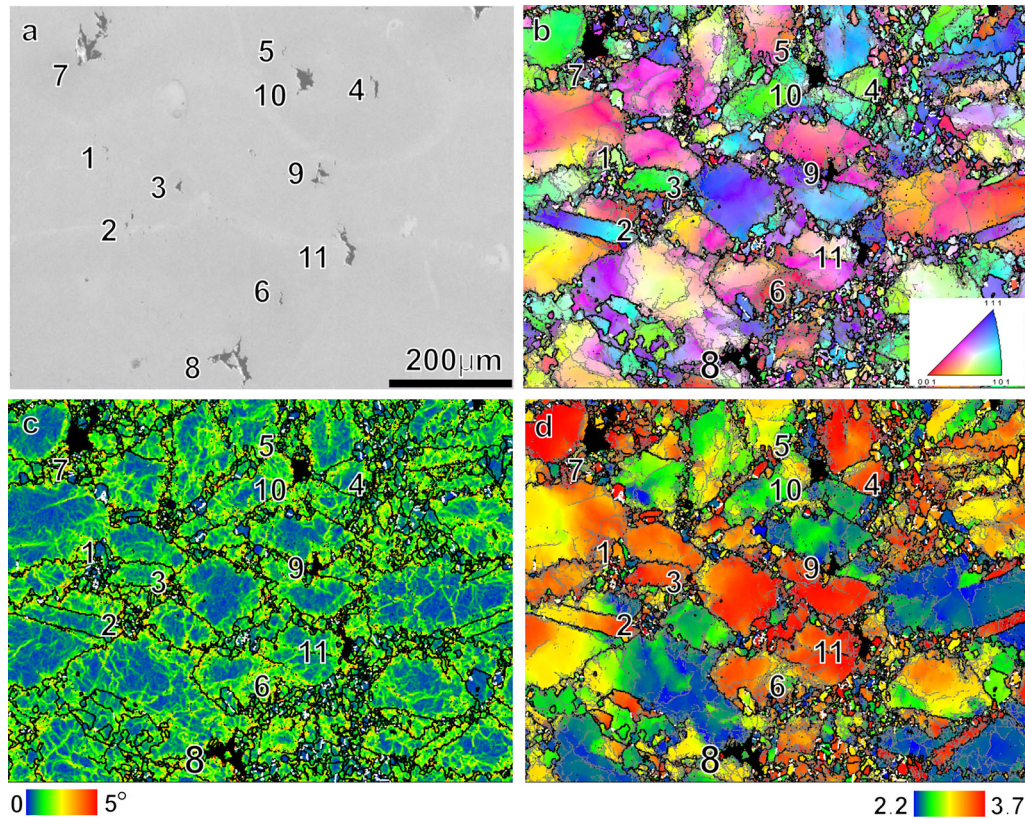


Fig. 10—(a) SEM image of the specimen tensioned at 1273 K (1000 °C) and 0.001 s^{-1} to a strain of 0.3; (b) corresponding IPF map; (c) KAM map; and (d) Taylor factor map.

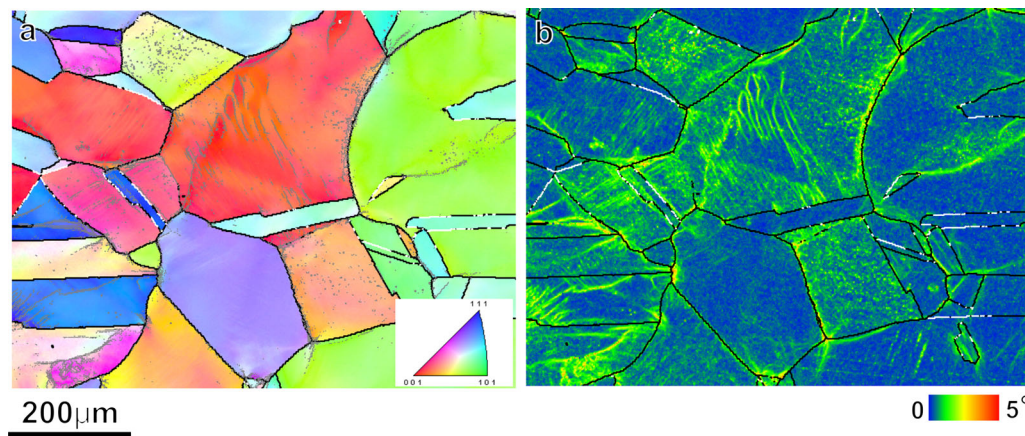


Fig. 11—(a) IPF map of the specimen tensioned at 1173 K (900 °C) and 10 s^{-1} to a strain of 0.2 and (b) corresponding KAM map.

at lower strain rates (Figures 6 and 7, 11, and 12). For this reason, the hot ductility increases with increasing strain rate at 1273 K and 1173 K (1000 °C and 900 °C). In addition, the effect of necking DRX on the deformation mechanism may be different to the conventional mechanism. It has previously been found that the strain rate sensitivity is indicative of superplastic flow in the recrystallized volume^[27] and may be related to flow instability.^[4]

The effect of the strain rate and necking DRX on the dislocation distribution at lower temperature [e.g.,

1273 K (1000 °C)] is represented in Figure 16. At high strain rates, the dislocation distribution becomes more uniform and the dislocation density increases with increasing strain. In contrast, at lower strain rates, greater strain concentration occurs near the GBs and the dislocation density within the grains is low. At sufficiently high strain, necking DRX occurs. Fine grains have lower deformation resistance than coarse grains.^[7] Furthermore, the newly formed DRX grains contain few dislocations. A large dislocation density gradient forms between the strained parent grains and

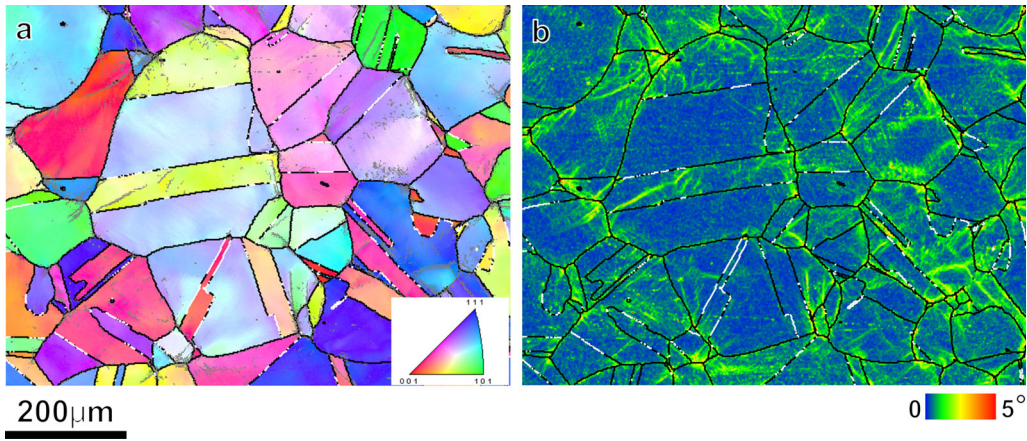


Fig. 12—(a) IPF map of the specimen tensioned at 1173 K (900 °C) and 0.1 s^{-1} to a strain of 0.2 and (b) corresponding KAM map.

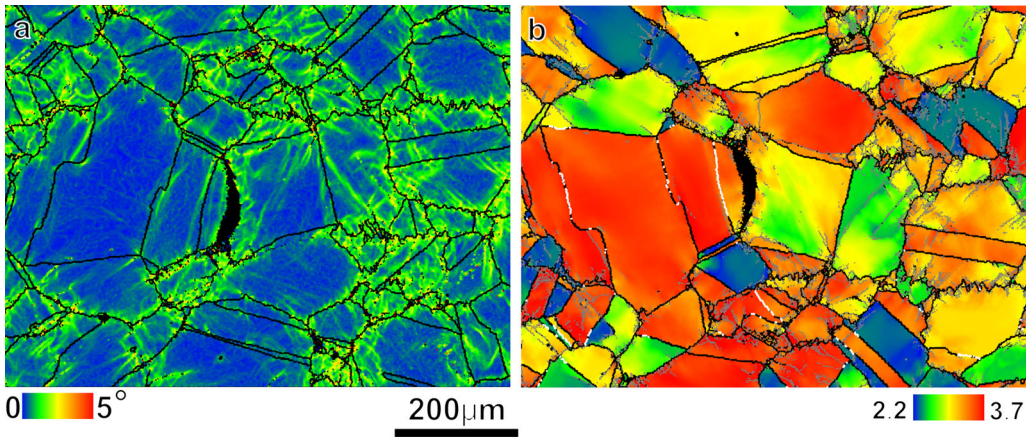


Fig. 13—(a) KAM map of the specimen tensioned at 1173 K (900 °C) and 0.001 s^{-1} to a strain of 0.2 and (b) corresponding Taylor factor map.

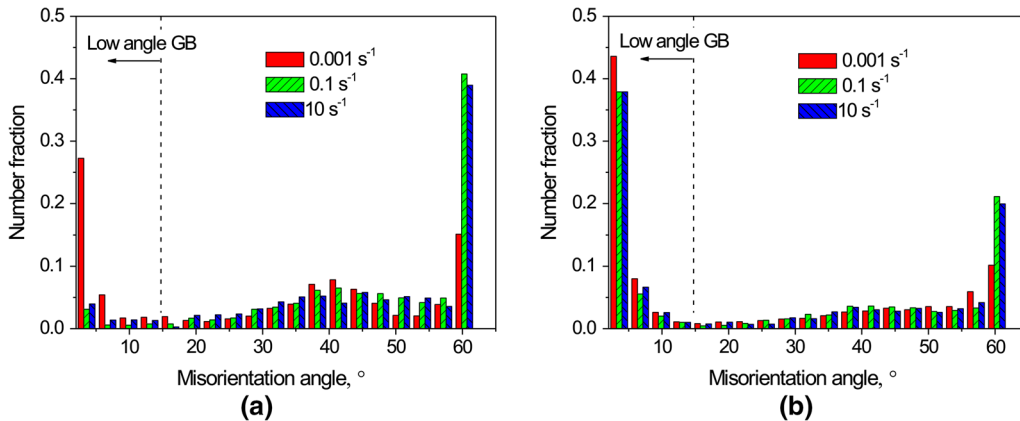


Fig. 14—Distribution of misorientation angles in specimens deformed at (a) 1473 K (1200 °C) and (b) 1373 K (1100 °C).

DRX grains, which promotes stress concentration and crack nucleation. Evidence for this is provided by the microstructure in Figure 17. The crack nucleation sites (indicated by the red arrows) are primarily between “hard” parent grains and “soft” necklace DRX grains. In this study, necklace DRX occurs during tension. During compression, the global stress states will

be different, which may affect the role of necklace DRX.

C. Grain Boundary Sliding

It has been reported that cracks formed along austenite GBs can be caused by GB sliding.^[30] However,

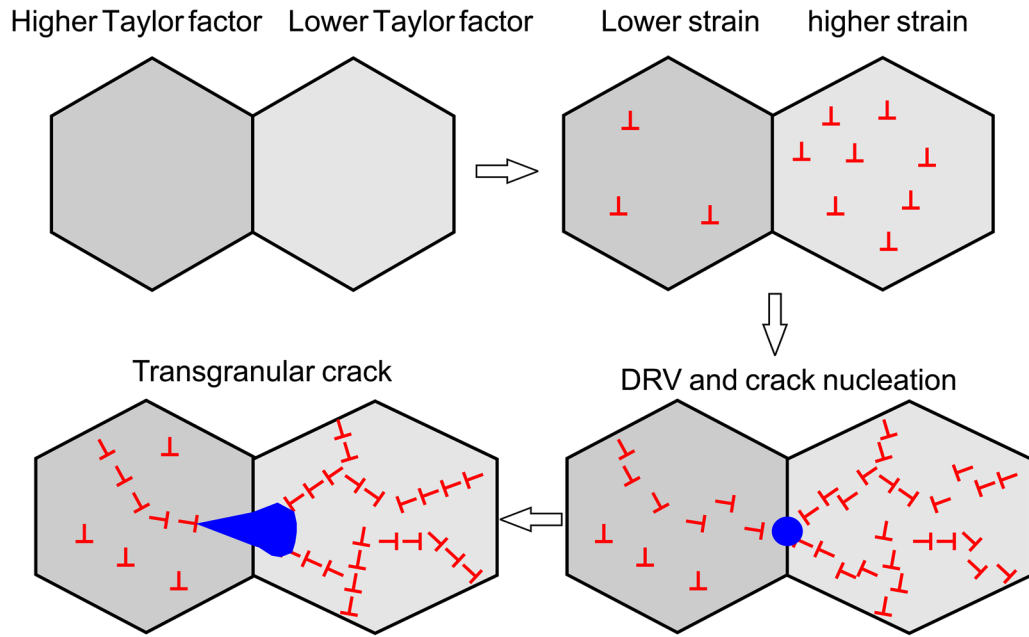


Fig. 15—Schematic illustration of cracking under a very low strain rate (e.g., 0.001 s^{-1}) and high deformation temperature [e.g., 1473 K (1200 °C)]. The dislocations are shown in red and the cracks are shown in blue.

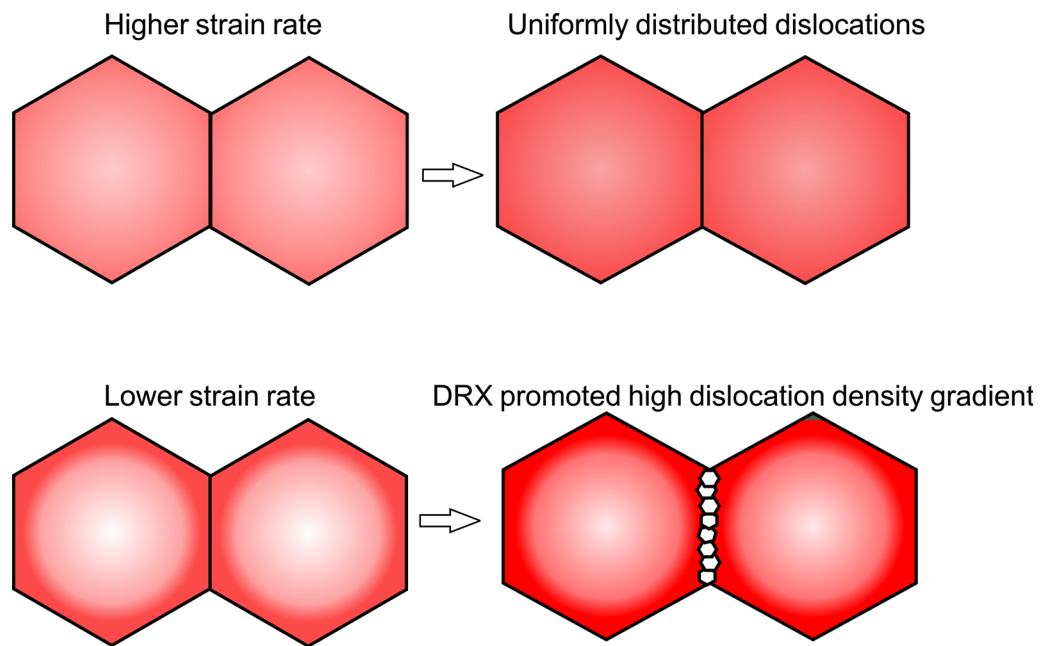


Fig. 16—Schematic illustration of the effect of strain rate and DRX on the dislocation distribution at lower temperature [e.g., 1273 K (1000 °C)]. Dark shading denotes higher dislocation density.

GB sliding is also thought to be a basic deformation mechanism rather than an effective embrittling mechanism at low strains.^[31] The role of GB sliding in the deformation of metallic materials is still under debate.

Figure 18 shows the results from the specimen tensioned at 1273 K (1000 °C) and 0.001 s^{-1} to a strain of 0.3. A small crack can be seen in front of a large crack. The matrix between them remains unbroken and DRX occurred in this unbroken region (Figure 18(b)). The DRX grains and cracks are located between two grains

with high Taylor factors. “Hard” grains will rotate to a “soft” orientation to accommodate deformation during tension, resulting in a wedge-type crack. DRX grains were induced by GB sliding, in the form of local shear deformation in the narrow regions near the GBs. GB sliding is an accompanying phenomenon of grain rotation, and under these deformation conditions, it does not induce cracking; rather, cracking is caused by incompatible deformation between adjacent grains and grain rotation.

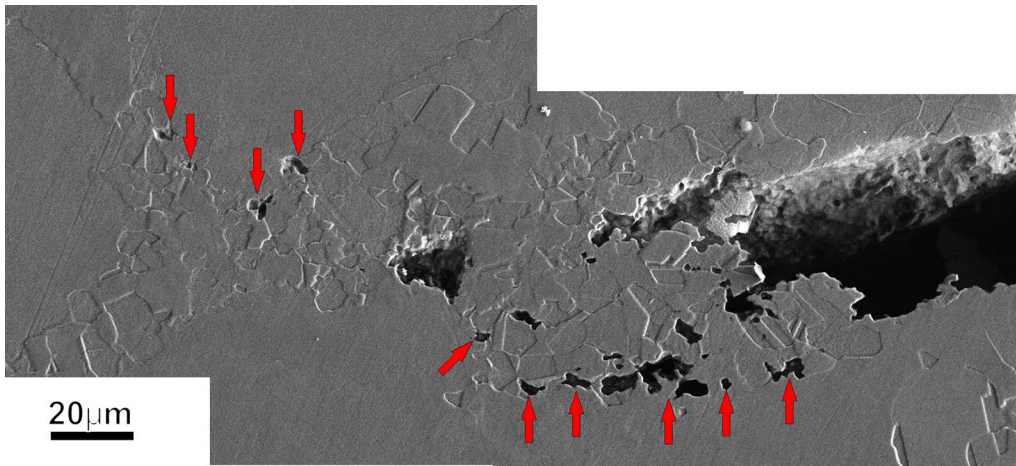


Fig. 17—SEM image of the specimen tensioned at 1273 K (1000 °C) and 0.001 s^{-1} to a strain of 0.3.

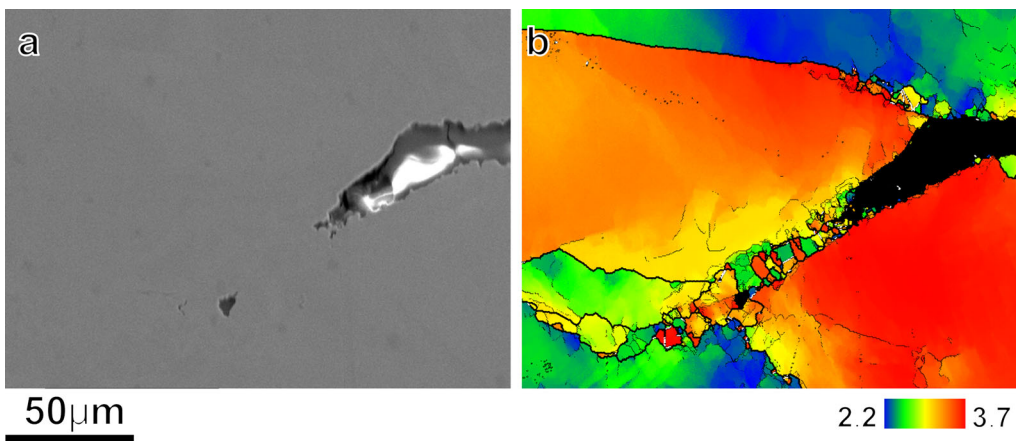


Fig. 18—(a) SEM image of the specimen tensioned at 1273 K (1000 °C) and 0.001 s^{-1} to a strain of 0.3 and (b) corresponding Taylor factor map.

D. Role of Strain Rate in Hot Cracking

A higher strain rate leads to a more uniform strain distribution, finer DRX grains, and more DRV inhibition, thereby allowing good hot ductility to be achieved. However, a higher strain rate leads to a lower extent of DRX and shear bands, which promotes hot cracking. The effect of strain rate on hot cracking depends on the microstructure evolution. If there is a balance between detrimental and beneficial microstructure evolution mechanisms and/or the change in strain rate is small,^[15] the strain rate effect will not be significant. Failure criteria for hot cracking modeling must include the microstructure evolution influenced by the strain rate rather than the strain rate itself.

It should be noted that, we did not consider several important factors in this study, such as the nitrogen content, intergranular precipitation,^[9,10] intragranular precipitation.^[52] Moreover, owing to instrumental limitations, experiments were not able to be conducted at strain rates higher than 10 s^{-1} . The strain rate effect on hot ductility at strain rates higher than 10 s^{-1} will be investigated using plane strain compression testing or

other more powerful equipments as a special topic in the further work.

V. CONCLUSIONS

1. The crack nucleation sites are primarily located at GBs and are unaffected by the strain rate at various deformation temperatures.
2. At high deformation temperature (1473 K (1200 °C)), a higher strain rate is beneficial for grain refinement and to prevent hot cracking; however, at very low strain rates (0.001 s^{-1}), DRV occurs and crack propagation is transgranular and along low-angle GBs.
3. At an intermediate deformation temperature [1373 K (1100 °C)], a high DRX extent and fine DRX grains at medium strain rate leads to good hot ductility.
4. The strain gradient from the grain interior to the GB increases with decreasing strain rate at low temperatures [1173 K to 1273 K (900 °C to 1000 °C)], which lowers the hot ductility.

5. GB sliding accompanies grain rotation and does not reduce the hot ductility.

ACKNOWLEDGMENTS

This project is supported by National Natural Science Foundation of China (Grant No. 51505416), the Natural Science Foundation—Steel and Iron Foundation of Hebei Province (E2013203110)—and the Foundation for Young Scholars in Yanshan University (14LGA004).

REFERENCES

1. J.W. Simmons: *Mater. Sci. Eng. A*, 1996, vol. 207, pp. 159–69.
2. J.W. Simmons: *Metall. Mater. Trans. A*, 1995, vol. 26A, pp. 156–60.
3. R.D. Knutsen, C.I. Lang, and J.A. Basson: *Acta Mater.*, 2004, vol. 52, pp. 2407–17.
4. Z.H. Wang, W.T. Fu, S.H. Sun, H. Li, Z.Q. Lv, and D.L. Zhao: *Metall. Mater. Trans. A*, 2010, vol. 41A, pp. 1025–32.
5. Z.H. Wang, S.H. Sun, B. Wang, Z.P. Shi, and W.T. Fu: *Mater. Sci. Eng. A*, 2015, vol. 625, pp. 321–30.
6. Z.H. Wang, W.T. Fu, S.H. Sun, Z.Q. Lv, and W.H. Zhang: *J. Mater. Sci. Technol.*, 2010, vol. 26, pp. 798–802.
7. Z.H. Wang, S.H. Sun, B. Wang, Z.P. Shi, R.H. Zhang, and W.T. Fu: *Metall. Mater. Trans. A*, 2014, vol. 45A, pp. 3631–39.
8. R.D. Doherty, D.A. Hughes, F.J. Humphreys, J.J. Jonas, D. Juul Jensen, M.E. Kassner, W.E. King, T.R. McNelley, H.J. McQueen, and A.D. Rollett: *Mater. Sci. Eng. A*, 1997, vol. 238, pp. 219–74.
9. J. Moon, T.H. Lee, J.H. Shin, and J.W. Lee: *Mater. Sci. Eng. A*, 2014, vol. 594, pp. 302–08.
10. E. Erisir, U. Prael, and W. Bleck: *Mater. Sci. Eng. A*, 2010, vol. 528, pp. 519–25.
11. J. Deng, Y.C. Lin, S.S. Li, J. Chen, and Y. Ding: *Mater. Design*, 2013, vol. 49, pp. 209–09.
12. S.W. Kim and Y.S. Lee: *Metall. Mater. Trans. B*, 2014, vol. 45B, pp. 445–53.
13. J. Liu, L.H. Qi, P. Liu, J.T. Guan, and J.M. Zhou: *Mater. Sci. Eng. A*, 2014, vol. 596, pp. 157–64.
14. O. Sabokpa, A. Zarei-Hanzaki, and H.R. Abedi: *Mater. Sci. Eng. A*, 2012, vol. 550, pp. 31–38.
15. S.P. Tan, Z.H. Wang, S.C. Cheng, Z.D. Liu, J.C. Han, and W.T. Fu: *Mater. Sci. Eng. A*, 2009, vol. 517, pp. 312–15.
16. J.L. He, Z.S. Cui, F. Chen, Y.H. Xiao, and L.Q. Ruan: *Mater. Design*, 2013, vol. 52, pp. 547–55.
17. M. Faccoli and R. Roberti: *J. Mater. Sci.*, 2013, vol. 48, pp. 5196–23.
18. E. Hurtado-Delgado and R.D. Morales: *Metall. Mater. Trans. B*, 2001, vol. 32B, pp. 919–27.
19. G.Q. Hou, L. Zhu, H.X. Bian, and Y.L. Tian: *Chin. J. Mater. Res.*, 2013, vol. 27, pp. 70–74 (in Chinese).
20. X.W. Duan and J.S. Liu: *Mater. Sci. Eng. A*, 2013, vol. 588, pp. 265–71.
21. X.P. Wei, W.W. He, and J.S. Liu: *J. Taiyuan Univ. Sci. Technol.*, 2012, vol. 31, pp. 296–99 (in Chinese).
22. H.J. McQueen: *Metall. Mater. Trans. A*, 2002, vol. 33A, pp. 345–62.
23. I. Bantounas, T.C. Lindley, D. Rugg, and D. Dye: *Acta Mater.*, 2007, vol. 55, pp. 5655–65.
24. N. Subrahmanya Prasad, N. Naveen Kumar, R. Narasimhan, and S. Suwas: *Acta Mater.*, 2015, vol. 94, pp. 281–93.
25. A. Clair, M. Foucault, O. Calonne, and E. Finot: *Scripta Mater.*, 2014, vol. 82, pp. 21–24.
26. W.H. Zhang, S.H. Sun, D.L. Zhao, B.Z. Wang, Z.H. Wang, and W.T. Fu: *Mater. Design*, 2011, vol. 32, pp. 4173–79.
27. D. Ponge and G. Gottstein: *Acta Mater.*, 1998, vol. 46, pp. 69–80.
28. S. Kibey, J.B. Liu, M.J. Curtis, D.D. Johnson, and H. Sehitoglu: *Acta Mater.*, 2006, vol. 54, pp. 2991–3001.
29. F.J. Humphreys and M. Hatherly: *Recrystallization and Related Annealing Phenomena*, 2nd ed., Elsevier, Oxford, 2004, p. 131.
30. B. Mintz: *ISIJ Int.*, 1999, vol. 39, pp. 833–55.
31. F. Zarandi and S. Yue: *Metall. Mater. Trans. A*, 2004, vol. 35A, pp. 3823–32.
32. M.H. Kang, J.S. Lee, Y.M. Koo, S.J. Kim, and N.H. Heo: *Metall. Mater. Trans. A*, 2014, vol. 45A, pp. 4302–06.